THE UNIVERSITY of EDINBURGH

Edinburgh Research Explorer

On the interest of studying degradation gases for forest fuel combustion modeling

A comparison between three time-varying, axisymmetric, non-premixed, laminar flames of forest fuels

VIRGINIE TIHAY[a], ALBERT SIMEONI[a], PAUL-ANTOINE SANTONI[a], LUCILE ROSSI[a], VERONIQUE BERTIN[b], LAURENCE BONNEAU[b], JEAN-PIERRE GARO[b] AND JEAN-PIERRE VANTELON[b]

[a]SPE– UMR 6134 CNRS, University of Corsica, Campus Grossetti, BP 52, 20250 Corte, France Phone: (33) 495 450 121; Fax: (33) 495 450 162

[b]LCD – UPR 9028 CNRS, ENSMA, University of Poitiers, 1 avenue Clément Ader, Téléport 2 – BP 40109, 86961 Futuroscope Chasseneuil Cédex, France

Abstract – To simulate the spreading of wildland fires at the field scale, there is a need of simple models for gas oxidation. The aim of this work is to provide such a model. To proceed, a laboratory experimental apparatus was designed to generate laminar, axisymmetric, time-varying and non-premixed flames of three different pine needles. The distribution of temperature was characterized in the flame, as well as the mass loss, the flame height and the flame radius, showing very different flame behaviours. The gases released from the pyrolysis of one of the fuels were analysed thanks to a tube furnace apparatus connected to a gas chromatograph The experimental data were used to propose a simple formulation for fuel oxidation. It was included in a numerical model solving the reactive and radiative flow equations. The calculated distribution of temperature in the flame does agree with the experimental one, validating the oxidation model.

Keywords: laminar diffusion flame; wildland fire; gas oxidation model

INTRODUCTION

Devastating fires regularly damage all continents over the world. Under these circumstances, it would be very useful to have a predictive tool that can be used for management of forest fire. In light of this, the scientific community has become increasingly involved in both modelling and experimental areas for forest fire. Beginning in North America and Australia fifty years ago [1-3], a number of modelling approaches have emerged. Three types of models can be identified [4]. The first one includes statistical models [5]. The second one incorporates empirical models [2]. Based on a detailed description of the heat transfer mechanisms which govern the fire propagation, the physical models [6-8] are the third set of models. Among them the two-phase models consider a gas phase flowing through a bed of fuel particles. However, gases combustion is poorly modelled in those approaches. The combustible part of the devolatilization products is considered to be solely carbon monoxide that burns in air [8], whatever be species and elements composing actual vegetation. Global rate and thermodynamic parameters are included in the model for this representative fuel and oxidizer pair. However, wood is a complex material and the mixture composition of its degradation gases changes with different vegetative species [9].

The effective variability in the amount and composition of these gases as well as the need for a simple reliable model [10] for their oxidation to be included in a model of wildand fire has motivated this work. Based on study of the gases released from the degradation of pine needles, a very simple formulation for fuel oxidation is provided. To proceed, the structure of an unsteady, axisymmetric, non-premixed laminar flame of pine needles is investigated computationally and experimentally. An original experimental device was built in order to generate such a flame. Time-varying laminar diffusion flame is a class of non-premixed combustion bridging the gap [11] between

steady laminar combustion and turbulent combustion encountered in forest fire. Experimentally, the distribution of temperature along the fire plume and the plume as well as the mass loss are measured and compared for three different pines' needles. The gases released by the degradation of the pine needles were determined by using a tube furnace connected to a gas chromatograph. Four main pyrolysis gases (carbon monoxide CO, methane CH4, hydrogen H2 and carbon dioxide CO2) were identified from this degradation. A primitive variable formulation was used to solve the transient conservation equations of mass, momentum, energy, species as well as radiation. Predicted and measured temperature along the flame axis was compared at different time during the decreasing flame activity for one of the three forest fuels investigated. The experimental procedures are described in the following section. Next, the model and the numerical method are presented. Finally, results are discussed and concluded.

EXPERIMENTAL DEVICES AND METHODS

Analysis of the pyrolysis gases

The tube furnace apparatus used as pyrolyser is shown in Fig. 1. It is made of a cylindrical furnace 43.5 cm long with an internal diameter of 6.5 cm. The reactor inside, is 86 cm long with an inner diameter of 5 cm. Two thermocouples were used to record the temperature history in the furnace. One was fixed on the inner surface of the furnace and the other was placed in the middle of the combustion boat. Experiments were conducted with needles of *Pinus laricio*, an endemic pine of Corsica. Before experiments, pine needles were oven dried at 60°C for 24 hours. Fuel was then crushed and sieved to a particle size of 0.6-0.8 mm. Different ranges of temperature were used to pyrolyse the fuel: 290 to 425°C, 500 to 600°C and 600 to 700°C. The temperature of the furnace was set, for these three ranges respectively at 450°C, 600°C and 700°C. Gases

were collected into two balloons called the gas sampler hereafter. The combustion boat filled with 4 g of crushed pine needles was kept outside of the furnace until the temperature of the furnace has reached the required value. At the same time, air suction was switched on, the gas sampler was opened and nitrogen was injected at 1 L/min to obtain an inert atmosphere in the device. When the temperature was stable, the sample was introduced inside the furnace. The injection of nitrogen was stopped, gas sampler was closed and the valve (8a on Fig. 1) allowing the ejection of gases outside the apparatus was opened. When pine needles reached the required temperature, gas sampling began. Valve 8a was closed, a gas sampler was opened and nitrogen was injected into the reactor to fill the gas sampler with pyrolysis gases. Then the gas sampler was directly attached to the gas chromatograph (Flame Ionization Detector and Thermal Conductivity Detector). The sample of pine needles was gone out the furnace and a load cell was used to obtain the mass loss. For each range of temperature, at least three repetitions were carried out.

Time-varying, axisymmetric, diffusion flame

The experimental device is shown in Fig. 2. The bench of combustion was composed of a one square meter plate drilled at its centre. A ten square centimetres insulator was included at this location to support the fuel. It was positioned on a load cell in order to measure the fuel mass loss as a function of time. To insure a fast and homogeneous ignition, a small amount of ethanol (0.3 mL) was spread uniformly on the fuel bed and was ignited with a flame torch. A refined study was conducted to achieve a size and a shape for the fuel bed as well as a size for the particles to be burned, allowing to generate a time-varying, axisymmetric, and laminar diffusion flame. An array of 11 thermocouples was positioned above the fuel bed along the flame axis. The first

thermocouple was placed 1 cm above the top of the support and the others were located 1 cm from each other. The thermocouples used were mineral-insulated integrally metal-sheathed pre-welded type K (chromel-alumel) pairs of wire with an exposed junction. At the exposed junctions the wires were 50 mm in diameter. The load cell was chosen for his very short response time (0.2 s) compared to the conventional techniques (analytical balances) which have a response time greater than 3 s. The uncertainty in temperature and mass measurements were respectively 0.5°C and 0.1 g. The sampling frequency was 100 Hz. A visual camera located on the side showed that the device effect on the hydrodynamics was negligible. A second visual camera was placed above the flame in order to observe the regression of the flame basis. Burnings were conducted with three different types of oven-dried and crushed pine needles from Pinus laricio, Pinus halepensis and Pinus pinaster (all particles sizes of 0.6-0.8 mm). The beds of fuel were in the shape of a disk with a diameter of 3.5 cm, a depth of 0.5 mm and a mass of 1.5 g.

Image processing

An automatic algorithm was carried out in order to follow the flame height and the width of the flame basis (camera 1 and 2 in Fig. 2, respectively) as a function of time. Images were first extracted from videos with a sampling rate of 0.5 Hz. For each image, the flame was segmented from the background by using selection criteria based on the RGB components. The first step of the pixel extraction was the selection of pixels with a high magnitude in the red component. In the second step, only the pixels with a certain gap between the red and blue components and the red and green components were kept. This avoided the selection of pixels whose colour is due to light effects. Binary images results from this processing, showed in white colour the segmented

flame on the image plane. Next, the flame height and the width of the flame basis were computed using the Cartesian coordinates of the white area in the image plane. For the frontal view, the height of the flame corresponded to the height of the white area. In the case of top vision, the width of the flame basis was the average diameter of the white area.

NUMERICAL SOLUTION

As this paper is focused on the gas oxidation, the combustion of the vegetative fuel is simplified: the gas and solid phase's interchanges are not considered and the rate of the degradation products entering the gas phase is modelled by a burner. The numerical model solves the two-dimensional, axisymmetric, time-dependant, reactive-flow Navier-Stokes equations coupled with radiation and transport:

$$\frac{\partial \rho}{\partial t} + \vec{\nabla} \rho \vec{V} = 0 \tag{1}$$

$$\frac{\partial \rho Y_i}{\partial t} + \rho \vec{V}.\vec{\nabla} Y_i = \vec{\nabla}\left(\rho D_{ij} \vec{\nabla} Y_i\right) + \dot{\omega}_i \tag{2}$$

$$\frac{\partial \rho \vec{V}}{\partial t} + \rho \vec{V} \vec{\nabla}.\vec{V} = \vec{\nabla} p + \rho \vec{g} + \vec{\nabla}.\bar{\bar{\tau}} \tag{3}$$

$$\frac{\partial \rho e}{\partial t} + \rho \vec{V}.\vec{\nabla} e = \vec{\nabla}\left(\lambda \vec{\nabla} T\right) + \vec{\nabla}.\vec{R}_g + \vec{\nabla}\left(\rho \sum_{i=1}^{N} h_i D_{ij} \vec{\nabla} Y_i\right) - \vec{\nabla}.\left(p \vec{V}\right) + \vec{\nabla}.\left(\bar{\bar{\tau}}.\vec{V}\right) + \dot{Q} \tag{4}$$

$$\frac{dI(\vec{r},\vec{s})}{ds} + a I(\vec{r},\vec{s}) = a \frac{\sigma T^4}{\pi} \tag{5}$$

The incompressible ideal-gas law is used to calculate density variations. An ideal gas mixing law defines the viscosity and the thermal conductivity of the mixture. The diffusion coefficients are computed using the kinetic theory (McGhee, 2000). A mixing

law defines the specific heat of the mixture. The bulk viscosity in the stress tensor is neglected. The scattering is neglected in the Radiative Transfer Equation (RTE) (Eq. 5). To obtain a simple model for radiation, the gas is approximated by a mixture of grey gases containing CO2 and H2O. The RTE is solved by using the Discrete Ordinates Method (DOM) (Chui and Raithby, 1993). The studied domain is discretized in 8 control angles. The governing equations for the gas phase are discretized on a non-uniform grid using a finite-volumes procedure. A first-order backward Euler scheme is used for time integration. Diffusion terms are approximated using a second-order central difference scheme. Convective terms are discretized using a first-order upwind scheme. The pressure-velocity coupling was handled by using the SIMPLE algorithm (Patankar, 1980). The resulting systems of linear algebraic equations are then solved iteratively by using the Algebraic Multigrid algorithm (Hutchinson and Raithby, 1986).

Global reactions based on Arrhenius laws were used for CH_4 and CO in order to simplify the combustion of the degradation gases. A single step mechanism was considered for the combustion of CO and a two-step mechanism was used for CH_4 (see Table 1). The second step for CH_4 corresponds to the combustion of CO. For full kinetics mechanisms, the values of the coefficients in the Arrhenius' formula are known for most of the elementary reactions. However, when global mechanisms are considered, the reaction rate parameters have to be fitted (Westbrook and Dryer, 1984). Their values depend on the laminar or turbulent pattern of the flow. In the present work, the activation energy of CO developed by Dryer and Glassman, (1973) for turbulent combustion was adapted to laminar combustion. This value was divided per 3.

RESULTS AND DISCUSSION

Degradation of Pinus laricio's needles in the tube furnace

Table 2 shows the main degradation gases analysed for the three ranges of temperature. The needles being ovendried before the experiments, water vapour was not investigated. Degradation gases mainly consist of CO_2, CO, CH_4, O_2 and lower amounts of H_2, C_2 and C_3 hydrocarbons. At low temperatures (below 425°C), CO_2 and CO are the main components. They represent respectively 80% and 13.8% of the whole gases. They come from the degradation of the extractives, the hemicellulose and from the first stage of the degradation of cellulose (Orfão et al., 1999, Várhegyi et al. 1997). As temperature reaches 350°C, the formation of tar vapour from cellulose becomes predominant due to the decrease of its degree of polymerization. A deposit of tar on the reactor outside the furnace confirms this result. As the temperature reaches 425°C and stays below 600°C, the composition of the degradation gases changes significantly. The mass fraction of CO_2 decreases with increasing temperature. Conversely the mass fractions of CO, CH_4 and O_2 increase (Fagbemi et al. 2001). Above 425°C, cellulose, hemicellulose and lignin degrade. However, cellulose and hemicellulose are at the end of their degradation stage whereas lignin attains its fastest rate of degradation. This last process is largely responsible for the evolution of CO_2 and the increase in O_2 between the ranges 290-425 and 500-600. Three tests without fuel were carried out to verify that the presence of O_2 was not caused by leaks in the experimental device.

Burning experiments

Several runs were conducted in an enclosure avoiding air motion. The ambient temperature was 21°C and the relative humidity was 50 %. The flame behaviour, the radius and the height of flame, the mass loss as well as the distribution of the vertical

temperature along the flame axis are discussed. The mass loss, the mean temperature at the top of the fuel bed and radius of the flame were used to implement the model. The vertical temperatures were used to test it. At least five repetitions were made for each variable to collect reliable data.

Flame behaviour

Figures 3 show the laminar flame of three species, 90 s after the ignition. The flame of *Pinus halepensis* is orange whereas the *Pinus pinaster* one is quasi blue. *Pinus laricio* has a halfway colour, with a blue region near the sample and an orange one at the top of the flame. The ability of *Pinus halepensis* to make soot may be higher than *Pinus laricio* and *Pinus pinaster* as the colour of orange region is related to soot radiation.

The same global behaviour was observed for all the pine species, including three different stages: ignition stage, laminar stage and extinction stage. The first stage corresponds to a low turbulent and flickering flame due to the presence of ethanol. During the second stage, the ethanol was completely burned and the combustible was only composed of the degradation gases. The flame became laminar (cf. Figs. 3) and decreased slowly. The last stage concerned the extinction of the flame. The remaining solid phase was essentially made up of carbon at the surface of the sample with a certain amount of unburned fuel near the support. A small (and negligible) amount of ashes at the surface is observed too.

Mass loss

For the three pines, the mean data provided by the load cell were interpolated thanks to 4th order polynomials (cf. Fig. 4), which are used in the simulation to set the mass flow

inlet of degradation gases. During the first 60 s, a steep decrease corresponding to the burning of ethanol is observed. Next, during the laminar flame stage, *Pinus halepensis* had the steepest slope followed by *Pinus laricio* and *Pinus pinaster*. Their global mass losses are 0.18, 0.25 and 0.27 g, respectively. These low values are due to the compactness of the crushed pine needles bed, avoiding the heat diffusion through the fuel bed.

Flame height

Figure 5 shows the flame height of the three pines in function to their mass flows. *Pinus halepensis* gives the highest flame following by *Pinus pinaster* and *Pinus laricio*, respectively. However, for a same mass flow, *Pinus halepensis* and *Pinus pinaster* have a close flame height whereas *Pinus laricio*'s one is about 1 cm lower.

Flame Radius

During the laminar stage, the mean radiuses of the flame basis were extrapolated for the three pines with quadratic polynomials. These polynomials are used in the simulation for setting the radius of the mass flow inlet zone. The flame base of *Pinus laricio* regresses faster than *Pinus halepensis* and *Pinus pinaster* ones, which regress similarly during the laminar stage. Next, the residence time of *Pinus laricio* flame is longer than the other species one due to a more in depth degradation of the sample.

According to the evolution of the flame height and the flame radius of the three pines, the combustion dynamics of *Pinus laricio* seems to be very different to the *Pinus halepensis* and *Pinus pinaster* one.

Vertical temperature

The vertical temperature follows the same trend for the three species. The mean time evolution of the temperatures for vertical thermocouples number 1, 2, 3, 4 and 7 are presented for *Pinus halepensis*, as they are representative of the fire plume (cf. Fig. 6). The first stage of the flame (presence of alcohol) lasts approximately 60 s and is not considered. During the second stage, the first three thermocouples take place inside the laminar flame, while the others are located above it. The temperature in the lower part is maximum reaching 1010°C for thermocouples 1, 2 and 3. The last region (above Th. 4) is the plume zone, where the temperature decreases progressively from 880°C to the ambient. The temperature fluctuates less in the flame than above it, where the flow becomes turbulent.

Although the global behaviour is the same for the whole species, some discrepancies are observed. The mean temperature curves at 2 cm, corresponding to the laminar flame are discussed for the three pine species (cf. Fig. 7). *Pinus laricio* and *Pinus halepensis* reach approximately the same temperature about 1000°C, whereas the temperature of *Pinus pinaster* is 25°C lower. *Pinus pinaster* curve increases and decreases more rapidly than the others. *Pinus laricio* and *Pinus halepensis* follow the same temperature increase but *Pinus laricio* burns longer. These discrepancies are linked to the different mass losses discussed previously.

Computational domain and boundary conditions

All the computations have been carried out using a Cartesian non-uniform grid with a width of 6 cm and a height of 15 cm. The grid contains 115190 cells with a mesh size of 0.2 mm respectively from $z = 0$ to 6 cm and from $r = 0$ to 6 cm along the vertical and

radial direction. In the remaining part of the grid, a dilatation ratio of 1.03 was applied along the height. Finer grids were tested to ensure that the numerical results were grid-independent. A compromise between computational time and accuracy led to a time step of 0.05 s. The simulation time is 70 s. The CPU time on a 3.2 GHz workstation is about 24 h. The following inputs are directly deduced from the experimental data:

- the mass flow inlet is fitted from the experimental rate of mass loss,

- the radius of the burner, decreasing with time, is deduced from video analysis,

- the temperature of the degradation gases at the inflow is set equal to 440°C, that is the mean value measured at the top of the fuel bed,

- the water fraction in moist air is $Y_{H_2O} = 0.011$.

Two gas mixtures were tested in this study (see Table 3). The values obtained in the tube furnace for the range of temperature 290–425 were used to define them. Thermocouples located inside the fuel bed showed that the needles' temperature was most of the time lower than 425°C. The first mixture only considers CO as combustible gas whereas the second mixture consists of CO and CH_4. For both mixtures, the mass fraction of CO_2 is taken to set the sum of all mass fractions equal to 1. For the computations, a preliminary stationary solution of the flow field was calculated without reaction. Next, the flame structure for an irreversible infinitely fast chemistry for a flame of CO/air was used to ignite the mixture. Finally the chemical reactions were turned on to provide the unsteady solution.

Comparison between experimental and numerical results

Figures 8 to 10 show the simulated and experimental temperatures during the regression stage, respectively at 1, 2 and 7 cm height. The numerical results correspond to the mixtures of degradation gases given in Table 3. Experimental data were collected from five runs. The decrease of the experimental temperature with time is due to the decrease of the flame. The simulated results present different behaviours for both mixtures in the flame region (Fig. 8 and 9). These differences vanish in the thermal plume where the gases are carried out without reaction (Fig. 10). At a height of 1 cm (cf. Fig. 8), all experimental temperatures increase at the beginning of the regression stage. The predictions for both mixtures overestimate the temperature in this region during the first 40 s of the regression stage. Moreover, mixture one containing solely CO fails to describe the increase in temperature during this stage. Conversely mixture two, containing CO and CH_4 is able to provide this tendency. Mixture one burns too early in the vicinity of the burner outlet. The prediction of the temperature decrease at the end of the regression stage depends on the mixture composition as well. At a height of 2 cm (Figs. 8), the simulated temperature obtained for mixture two, containing CO and CH_4, is roughly in agreement with experiment. Mixture one, containing solely CO, underestimates the experimental temperatures. The second step in the mechanism of combustion for mixture two makes CO to burn higher along the flame axis than for the one step mechanism used for mixture one. In that case, CO burns very close to the burner outlet. From the height of 4 cm, the experimental temperatures diminish drastically over the regression stage (more than 300°C at 4 cm high for instance). This region corresponds to the beginning of the thermal plume. All the predicted curves are close to the experimental ones. Fig. 10 only provides the results at 7 cm high to shorten the presentation. All simulated curves are slightly higher than the experimental ones.

These discrepancies could be due to two simplified modelling hypothesis. Firstly, only radiant heat losses due to CO_2 and H_2O were considered. Soot formation/oxidation was not taken into account. Secondly, the model is laminar on the whole domain, whereas the thermal plume becomes turbulent with height (Marcelli et al. 2004). The cooling of the fire plume due to entrainment and mixing of ambient air in the upper part may thus be underestimated in comparison with the experiments. In spite of this discrepancy, simulated and experimental curves follow accurately the same tendency. Considering the whole set of data, the results of simulation for the mixture of CH_4, CO, CO_2 and O_2 match better the experimental data than those resulting from the other mixture without methane (CO, CO_2 and O_2). Moreover, another simulation (not provided here) was made with a mixture which is consisted of a mass fraction $Y_{CO}=0.21$, what corresponds to the same heat release rate of the mixture two. The results of this simulation showed that the temperatures are overestimated by more than 300K in the fire plume. These first results demonstrate the need to include more species than CO in the global reactions mechanisms used in the two-phase models of wildland fire (Porterie et al., 2000). These species must be confirmed by further studies.

CONCLUSIONS

From the experimental point of view, the discrepancies between the burning of pine needles litters were previously attributed to the different surface-to-volume ratios of each species [15]. According to our results, this behaviour is also due to the various compositions of the degradation gases, since the differences occur with crushed samples too. This work will be carried on to determine the composition of the degradation gases of other species.

From the numerical point of view, the results are encouraging since the simulated temperatures along the flame axis match the observed ones. This work represents the first step for the integration of a gas oxidation model in a wildland fire modelling. Further studies are necessary to test this model for different fuels, both in laminar and turbulent condition, for static and spreading flames. The kinetics of degradation of the solid phase must be investigated too, to take into account the coupling between the flame structure and the solid phase.

NOMENCLATURE

a absorptivity

D mass diffusivity

e total energy

$\vec{g}$ acceleration due to gravity

h enthalpy

I radiant intensity

N number of species

p pressure

$\dot{Q}$ volumetric heat source

r radial coordinate

$\vec{r}$ direction vector

$\vec{R}$ radiant heat flux

R reaction rate

$\vec{s}$ unit vector along the radiant intensity path

T temperature

t time

$\vec{V}$ velocity

Y mass fraction of species

z axial coordinate

Greek symbols

λ thermal conductivity

μ viscosity

ρ density

$\bar{\bar{\tau}}$ viscous stress tensor

σ Stefan-Boltzmann constant

$\dot{\omega}$ mass rate of production

Subscripts

i species i

j species j

REFERENCES

Albini, F.A. (1986) *Combust. Sci. Tech.,* 45, 101-113.

Alén, R. Kuoppala, E. and Oesch, P. (1996) *J. of Anal. and Appl. Pyr.*, 36, 137-148.

Byram, G.M. (1959) in: K. P. Davis (Ed.) *Forest fire control and use*, McGraw-Hill Book Company, New York, pp. 61

Chui, E.H. and Raithby, G.D. (1993) *Num. Heat Trans. Part B*, 23, 269-288.

Dryer, F.L. and Glassman, I. (1973) *Proc. Combust. Inst,.* 14, 987-1003.

Emmons, H. (1965) *Proc. Combust. Inst.*, 10, 951-964.

Fagbemi, L. Khezami, L. and Capart R. (2001), *Appl. Energy*, 69, 293.

Hutchinson, B. R. and Raithby, G.D. (1986) *Num. Heat Trans,.* 9; 511-537.

Klose, W. Damm, S. and Wiest, W. (2000) Proc. Int. Symp. of Catal. and Thermochem. Conv. of Nat. Org. Polym.,4, 9-17.

McArthur, A.G. (1966) *Weather and grassland fire behaviour*, Leafter n°100, Australian Forest and Timber Bureau.

McGhee, H.A. (1991) *Molecular Engineering*., McGraw-Hill, New York, pp. 480.

Marcelli, T. Santoni, P. A. Simeoni, A. Leoni, E. and Porterie, B. (2004) Int. J. Wildland Fire, 13, 1.

Mohammed, R.K. Tanoff, A. Smooke, M.D. Schaffer, A.M. and Long, M.B. (1998) *Proc. Combust. Inst.*, 27, 693-702.

Orfão, J.J.M Antunes, F.J.A. and Figueiredo, J.L. (1999) *Fuel*, 78, 349-358.

Patankar, S.V. (1980) *Numerical Heat Transfer and Fluid Flow*. Hemisphere Publishing Corporation, Washington, D.C, pp. 197.

Porterie, B. Morvan, D. Loraud, J.C. and Larini, (2000) M. *Phys. Fluids*, 12, 1762-1781.

Rothermel, R.C. (1972) *A mathematical model for predicting fire spread in wildland fuels*, INT-115, USDA Forest Service.

Santoni, P.A. and Balbi, J.H. (1998) *Fire Safety J.,* 31, 201-225.

Várhegyi, G. Antal, M.J. Jakab, E. and Szabo, P. (1997) *J. of Anal. and Appl. Pyr,*. 42, 73-87

Weber, R.O. (1991) *Int. J. of Wildland Fire* 1 (4), 245-248.

Westbrook, C.K. and Dryer, F. (1984) *Prog. Energy Combust. Sci.*, 10, 1-57.

White, R.H. Dietenberger, M.A. (2001) *Encyclop. of Mat. Sci. and Technol*., pp. 9712-9716.

Zhou, X. and Mahalingam, S. (2001) *Combust. Sci. and Tech.*, 171, 39-70.

List of captions

Table 1. Global reactions used for the combustion of the degradation gases in air (units are kmoles, cubic meters, seconds and Kelvins)

Table 2. Mass fractions of the main pyrolysis gases released by the *Pinus laricio* needles

Table 3. Mass fractions of the different species at the burner outlet for the two mixtures tested
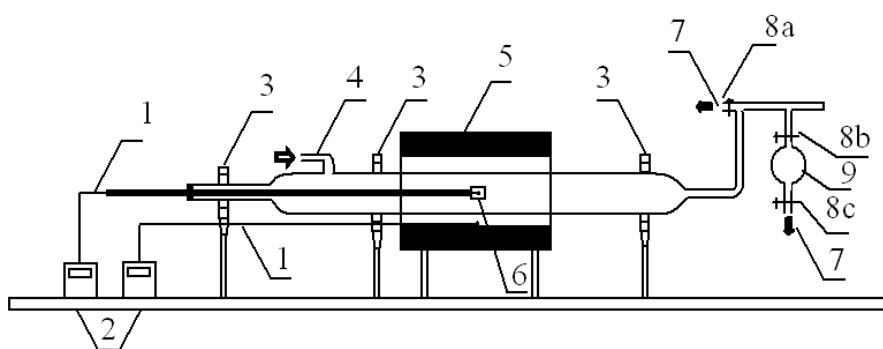
Fig. 1. Schematic of the tube furnace (1 thermocouple, 2 temperature controller, 3 bearing, 4 nitrogen injection, 5 electric furnace, 6 combustion boat, 7 air suction, 8a-c valves, 9 gas samplers).

Fig. 2. Sketch of the experimental apparatus.

Fig. 3. Flame shape at 90 s a) *Pinus halepensis* b) *Pinus pinaster* c) *Pinus laricio*.

Fig. 4. Mean mass loss for the three pines.

Fig. 5. Flame height of the three pines in function to their mass flows.

Fig. 6. Mean temperatures along the flame axis for *Pinus halepensis*.

Fig. 7. Mean temperature at 2 cm above the samples for the three pines.

Fig. 8. Observed and simulated temperature in function of time at a height of 1 cm.

Fig. 9. Observed and simulated temperature in function of time at a height of 2 cm.

Fig. 10. Observed and simulated temperature in function of time at a height of 7 cm.

Table 1. Global reactions used for the combustion of the degradation gases in air (units are kmoles, cubic meters, seconds and Kelvins)

CH$_4$ (1st step)	$CH_4 + 1.5O_2 \Rightarrow CO + 2H_2O$
	$R = 5.012 \times 10^{11} \exp(-24358/T)[CH_4]^{0.7}[O_2]^{0.8}$
CH$_4$ (2nd step)	$CO + 0.5O_2 \Rightarrow CO_2$
	$R = 2.239 \times 10^{12} \exp(-6495/T)[CO][H_2O]^{0.5}[O_2]^{0.25}$

Table 2. Mass fractions of the main pyrolysis gases released by the *Pinus laricio* needles

Species	Range of temperature (°C)		
	290 –425	500–600	600–700
	Mass fraction		
O_2	0.029	0.128	0.017
CO	0.138	0.208	0.306
CO_2	0.806	0.44	0.372
H_2	2.10^{-4}	0.006	0.02
CH_4	0.014	0.103	0.146
C_2H_4	0.004	0.041	0.073
C_2H_6	0.005	0.03	0.026
C_3H_6	0.004	0.043	0.042

Table 3. Mass fractions of the different species at the burner outlet for the two mixtures tested

Mixture n°	Y_{CO}	Y_{CH_4}	Y_{O_2}	Y_{CO_2}
1	0.138	0	0.029	0.833
2	0.138	0.014	0.029	0.819

Fig. 1. Schematic of the tube furnace (1 thermocouple, 2 temperature controller, 3 bearing, 4 nitrogen injection, 5 electric furnace, 6 combustion boat, 7 air suction, 8a-c valves, 9 gas samplers).

Fig. 2. Sketch of the experimental apparatus.

Fig. 3. Flame shape at 90 s a) *Pinus halepensis* b) *Pinus pinaster* c) *Pinus laricio*.

Fig. 4. Mean mass loss for the three pines.

Fig. 5. Flame height of the three pines in function to their mass flows.

Fig. 6. Mean temperatures along the flame axis for *Pinus halepensis*.

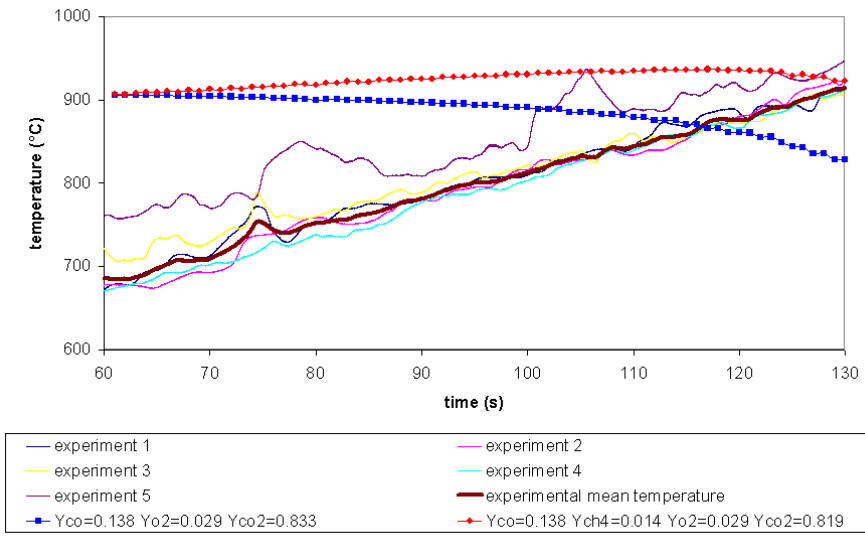Fig. 7. Mean temperature at 2 cm above the samples for the three pines.

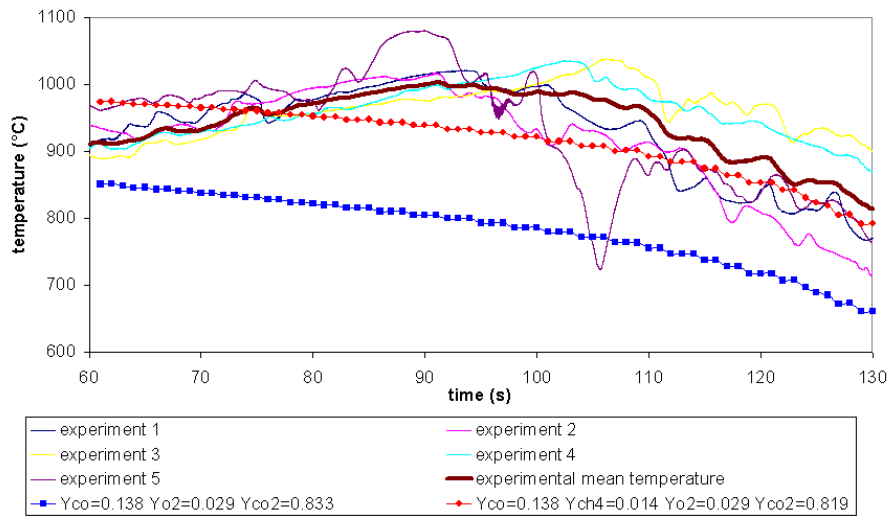Fig. 8. Observed and simulated temperature in function of time at a height of 1 cm.

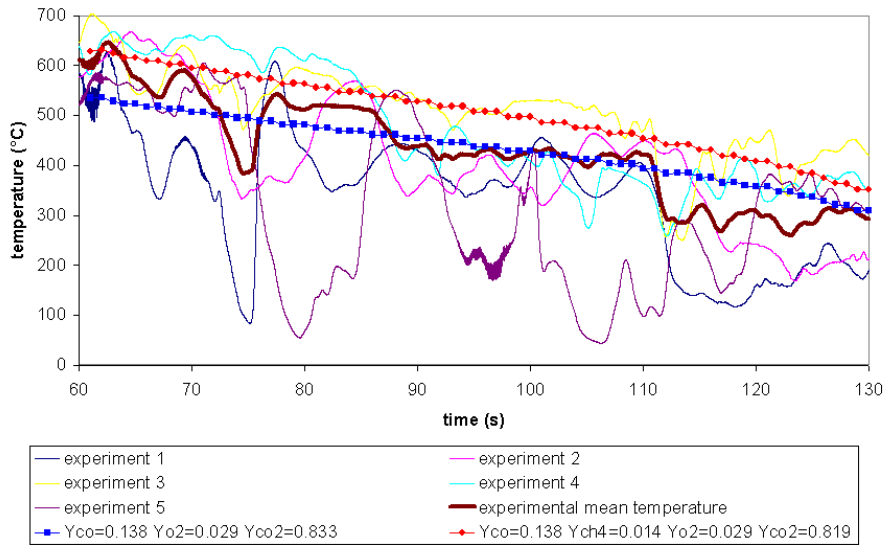Fig. 9. Observed and simulated temperature in function of time at a height of 2 cm.

Fig. 10. Observed and simulated temperature in function of time at a height of 7 cm.